

Effect of pre-deformation anneal on the microstructure and texture evolution of Mg–3Al–1Zn–0.7Sr alloy during hot extrusion

Alireza Sadeghi · Mihriban Pekguleryuz

Received: 12 October 2011 / Accepted: 14 March 2012 / Published online: 10 April 2012
© Springer Science+Business Media, LLC 2012

Abstract The effect of pre-deformation annealing on the microstructure and texture of an AZ31 + 0.74 wt% Sr alloy has been investigated. As-cast samples as well as three samples that have been annealed at 400 °C for 10, 30, and 120 min were extruded at 300 °C. Results indicate that annealing transforms the bulky non-equilibrium Al–Mg–Sr precipitates to stable Al₄Sr spheroids. As the extent of this transformation increases before extrusion, there is seen an increase in the amount of uniformly dispersed intermetallic stringers in the extruded material. Texture measurements reveal the alignment of basal poles with the compression axis (perpendicular to the circular cross section of the extruded bar) and the formation of the basal ring texture in all the samples. However, an increase in the duration of the pre-deformation anneal switches the plane facing the extrusion direction from first order prismatic (10–10) to second order prismatic planes (11–20). Annealing decreases the Al solute concentration in Mg and lowers the lattice resistance against dislocation movement. Consequently, the more favorable (0002)[11–20] slip system is activated in grains that see low basal resolved shear stress (τ). As a result, those grains work harden and are consumed by dynamic recrystallization (DRX). However, the (0002)[–1100] slip system with high τ still avoids basal dislocation movement. Hence, the grains with high $\tau_{(0002)[–1100]}$, which need to move dislocations in the (0002)[–1100] system to fulfill the strain compatibility conditions across the microstructure would be prevented from work hardening and DRX. This specific orientation has a (11–20) plane facing the extrusion direction.

Introduction

The design and development of high strength, formable, and isotropic wrought Mg alloys needed to manufacture automotive body parts such as door panels or front-end components has become the focus of much research. The addition of rare earth (RE) elements can be one of the routes to attain improved mechanical properties of Mg alloys [1, 2]. However, the high cost of the individual RE alloying additions limits the commercialization of those alloys [2], while using the more cost-effective mischmetal (combination of RE elements) can lead to microstructural instability. Strontium (Sr) has been added to the Mg alloys to achieve effects similar to RE elements properties of at lower price [3]. Sr additions have led to the development of the AJ series in 2002–2004 [3]. The alloy that was commercialized has considerable creep resistance, which makes it an excellent choice for powertrain applications [4, 5].

Strontium has also been added to work Mg alloys (AZ31 and M1) and the hot deformation behavior has been thoroughly studied [6–15]. Much work has been produced on the deformation of AZ31 [16–19] but the literature on AZ31 with Sr is scarce. The authors have previously reported that in AZ31 + Sr alloys, at specific thermo-mechanical conditions, thermally stable Al–Sr precipitates are able to initiate particle stimulated nucleation (PSN) and form grains with orientations other than the dominant basal texture [13, 14]. Nonetheless, there is an optimum level for Sr addition; excess levels of Sr will make the alloy brittle in deformation by inducing crack initiation at the Al–Sr precipitates [15]. Figure 1 shows how Sr influences the micro-mechanisms involved in the hot extrusion of AZ31–Sr alloys [14].

When Sr is added to AZ31 (Mg–3Al–1Zn), the formation of the β -Mg₁₇Al₁₂ precipitate is suppressed [6]. The

A. Sadeghi (✉) · M. Pekguleryuz
Department of Mining and Materials Science, McGill
University, Rm 2140, Wong Building, 3610 University Street,
Montreal, QC H3A 2B2, Canada
e-mail: alireza.sadeghi@mail.mcgill.ca

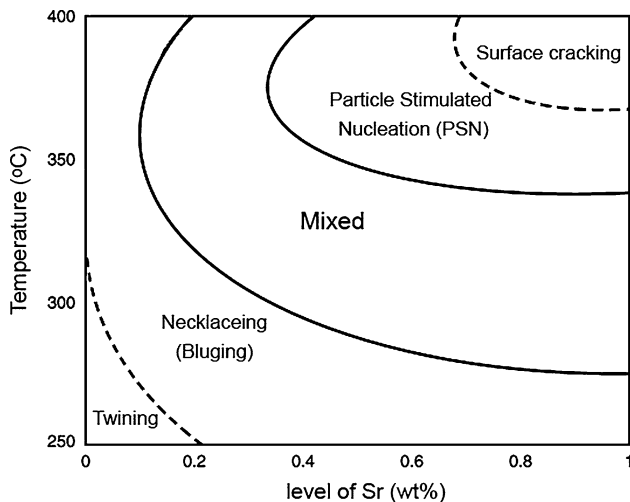


Fig. 1 Micro-mechanism map during extrusion of AZ31 alloy containing up to 1 % Sr at different temperatures [14]

equilibrium Al_4Sr precipitate formation is predicted [6, 7]. However, it is seen that, instead of the binary Al–Sr, a non-equilibrium ternary Al–Mg–Sr phase precipitates [7]. Janz et al. [20] have shown that the only ternary equilibrium precipitate in the Al–Mg–Sr system is $\tau\text{-Al}_{38}\text{Mg}_{58}\text{Sr}_4$, which is seen in alloys containing high levels of Sr and all other ternary precipitates are non-equilibrium. It has been reported by L'Espérance et al. [21] that the non-equilibrium Al–Mg–Sr precipitate rejects its excess Mg to the matrix and absorbs Al from the surroundings and decomposes to the equilibrium Mg– Al_4Sr eutectic. This decomposition has also been seen during the hot deformation of a cast alloy by the authors [15]. The unstable ternary precipitates can be partially or completely decomposed at different annealing times or temperatures. In the present research, four different Al–Mg–Sr/Al–Sr precipitate ratios have been prepared in AZ31 + 0.74Sr by controlling the annealing time and temperature. The as-cast and annealed samples were extruded at elevated temperatures and the final microstructure, precipitate distribution, hardness, and texture have been studied.

Experimental procedure

AZ31 extruded bars (provided by Applied Magnesium, Denver, CO) and Sr–10Al master alloy (Timminco, Haley, ON) were melted in a graphite crucible using a high frequency induction furnace (NORAX) at 700 °C to prepare the AZ31 + 0.74 wt% Sr alloy. The molten alloy was kept at 700 °C for 15 min to completely dissolve the master alloy. After skimming the melt surface, the temperature was raised to 720 °C then cast into a preheated cylindrical

steel die. The chemical composition of the cast sample was determined by inductively coupled plasma (ICP) and found to be Mg–3.07Al–0.843Zn–0.55Mn–0.74Sr.

Four samples were machined to cylinders 3 cm in diameter and 6 cm in height to fit the extrusion die chamber. Three samples were annealed at 400 °C for 10, 30, and 120 min using a Blue M Lindberg inert-gas mechanical convection-oven. The time and temperature values were selected based on the thermodynamic modeling of precipitation [6, 7], the selected values would insure a progressive series of partial and complete transformation of precipitates. Subsequently, the three annealed and the as-cast samples were extruded at 300 °C. Hot extrusion was performed using a steel-die setup (90° angle) and a 100 T hydraulic press down to a 1-cm diameter bar. The ram speed was kept constant at 4 mm/s and a high temperature anti-seize paste (Molycote P-37) was used for die lubrication. In order to achieve special combinations of precipitates, two more samples were also prepared. One of the samples was annealed at 250 °C and the other at 350 °C, both for 30 min and then extruded at their corresponding annealing temperatures.

The extruded bars were sectioned along the extrusion direction. The surface was prepared for optical and scanning electron microscopy by grinding and polishing with 1- μm diamond paste. Optical microscopy results were used to measure the grain size and the distance between the precipitate stringers by the line intercept method. Polished samples were examined using a back scattered electron detector (BSE) in a Hitachi S-4700 field emission gun scanning electron microscope (FEG/SEM). Electron probe microanalysis (EPMA) and electron back scatter diffraction (EBSD) was also performed to identify the phase compositions and element distribution and to investigate the misorientation inside the grains across the microstructure. Electro-polishing in a 5 % nital solution at 0 °C was used to prepare the EBSD samples and the grain structure was revealed using a picric acetic solution in optical microscopy.

Micro-Vickers hardness testing was performed on the extruded bars to investigate the hardness variation across the rectangular cross section. Measurements were carried out using 10-g force and in 0.5-mm intervals. Copper K_α X-rays were used in a D8 Bruker diffractometer to study the texture of the extruded samples. The beam was radiated on the center line of the rectangular cross sections with a 1-mm oscillation. The centerline of the sample has been selected to maintain identical location in all the samples. Orientation distribution functions (ODF), pole figures, and volume fraction of different planes in the extrusion direction were calculated from the raw data using the TextTools texture analysis software.

Results and discussion

Precipitates in as-cast and annealed microstructures

EPMA results of the as-cast AZ31 + 0.74Sr sample are shown in Fig. 2. The formation of the continuous precipitates at the grain boundaries and interdendritic regions can be easily distinguished in the back-scattered image and elemental maps. It is noted that the interdendritic precipitate contains Mg and confirms the formation of a ternary Al–Mg–Sr phase. Moreover, the existence of Zn is also observed in this phase. Interestingly, pure Zn has segregated to the interdendritic regions (the red color areas in the Zn map). This has been previously observed by the authors [7] and reported by other researchers [22]. The Mn map reveals the presence of needle shaped Al–Mn phase as well, which is known to be Al_8Mn_5 [7].

The BSE images of the as-cast and annealed precipitates are illustrated in Fig. 3. It is seen that increasing the annealing time at 400 °C up to 120 min (Fig. 3a–d) increases the fraction of the decomposed precipitate, which is identified via its spheroidized morphology. In Fig. 4, a partially decomposed Al–Mg–Sr precipitate is shown. As noted, upon thermal exposure, the non-equilibrium precipitate decomposes starting at its interface; by rejecting Mg and absorbing Al, the eutectic Al_4Sr precipitate is formed.

As seen in the optical micrographs of the extruded samples (Fig. 5), the non-annealed sample (Fig. 5a) has the finest grain size, and the final grain size of the alloy

increases with increasing annealing time before extrusion. The grain size values of the four extruded samples are graphically shown in Fig. 6. The increase in grain size with increasing annealing time can be attributed to two reasons:

- The size of the precipitates at the stringers is reduced and becomes less effective in blocking the movement of the grain boundaries and the growth of dynamically recrystallized grains.
- The Al–Mg–Sr \rightarrow Al–Sr transformation consumes Al atoms; as the dissolved Al in Mg solid solution decreases, the amount of Al atoms blocking dislocations at grain boundaries is reduced [13, 14].

It can be predicted that when the Al–Mg–Sr precipitates are completely decomposed to small spheroids, they could be dispersed more easily in the Mg matrix during extrusion. In Fig. 7a–d, the finer size of the precipitates and their more uniform distribution as a result of increasing annealing time can be seen. Measurements show that the average distance between the stringer lines has decreased by 39 %, from 23 to 14 μ m (Fig. 6) when the as-cast material has been annealed for 120 min. Fig. 8 shows the precipitate stringers in the samples annealed for 10 and 120 min at a higher magnification. It is observed that the precipitates in the sample annealed for 10 min (Fig. 8a) have also decomposed into spheroids, but the stringers are thicker compared to the sample annealed for 120 min (Fig. 8b). This decomposition occurs during hot deformation and is not able to disperse the spheroids homogeneously. The partial decomposition of the

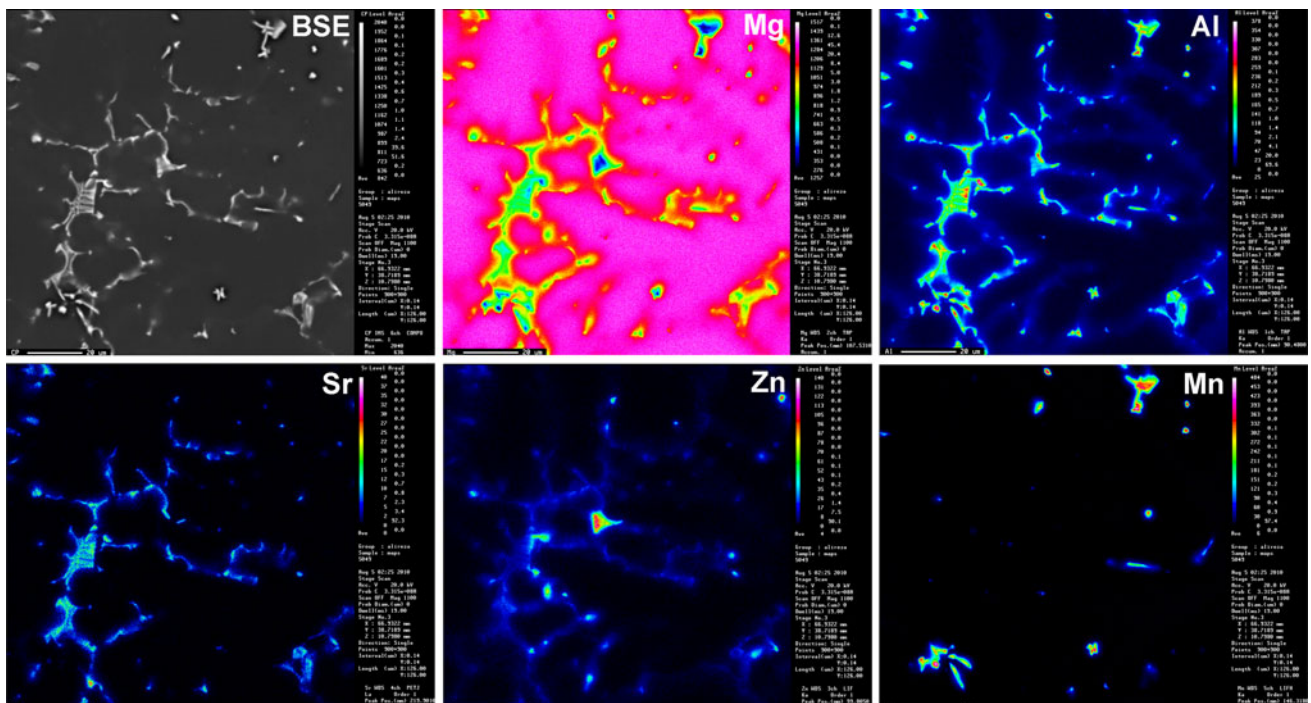


Fig. 2 EPMA mapping of as-cast AZ31 + 0.74 % Sr microstructure

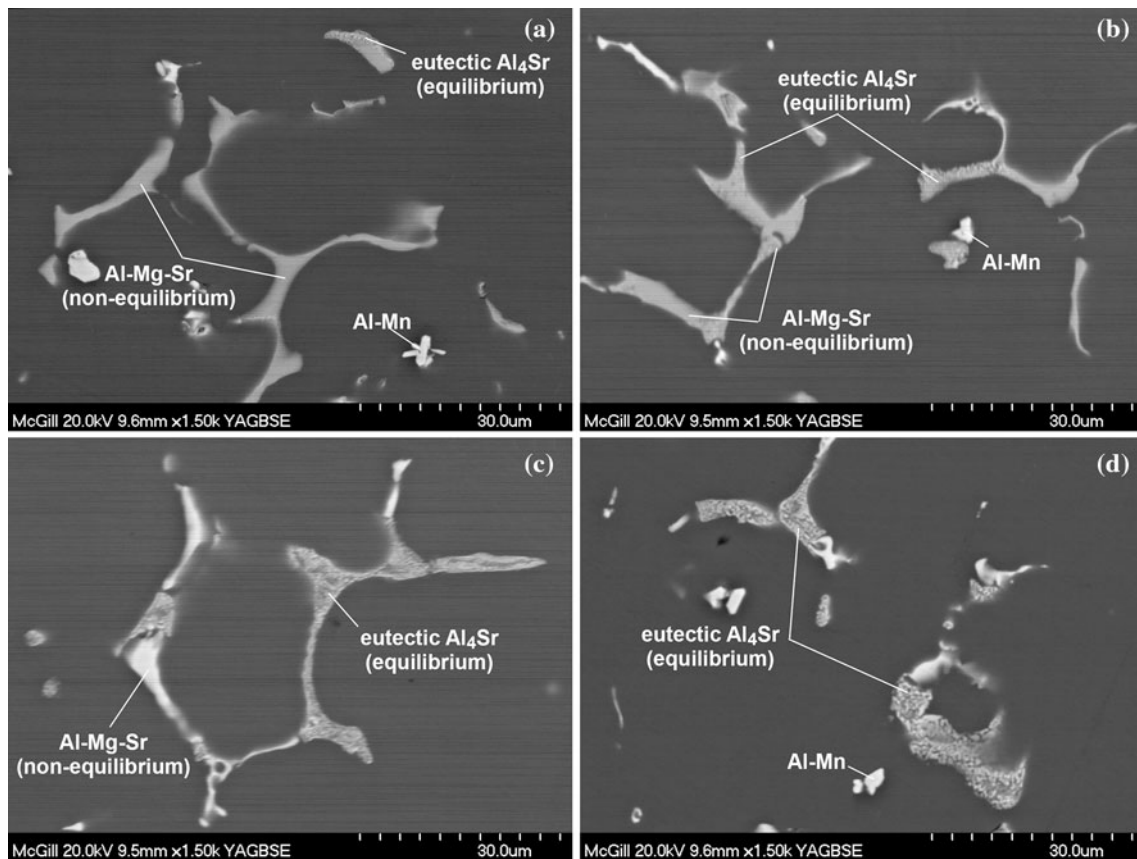


Fig. 3 Decomposition sequence of Al–Mg–Sr precipitate in AZ31 + 0.74 wt% Sr as a result of annealing at 400 °C, **a** as-cast, **b** 10 min, **c** 30 min, **d** 120 min

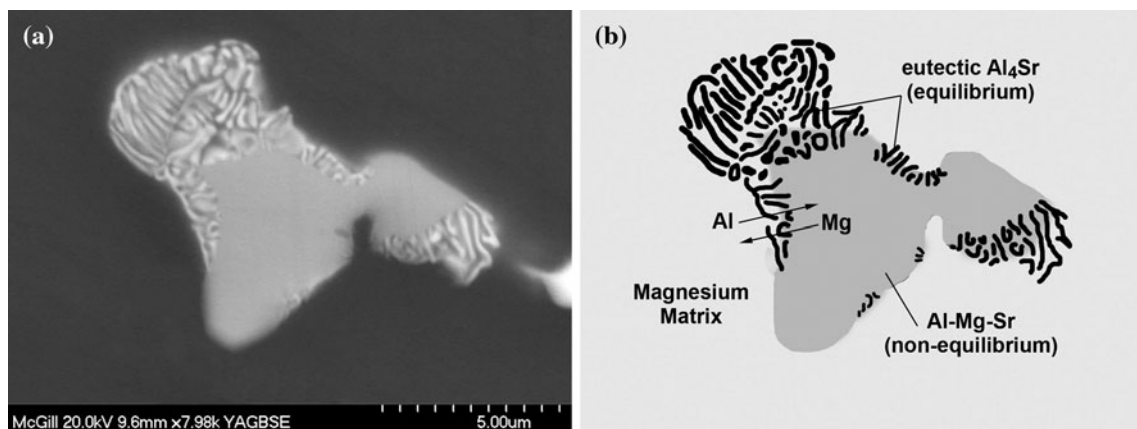


Fig. 4 Partial decomposition of an Mg–Al–Sr precipitate in as-cast AZ31 + 0.74 wt% Sr to laminar Al₄Sr precipitates

Al–Mg–Sr precipitates has been witnessed even in as-cast samples [15].

Cracking tendency of the precipitates

To investigate the cracking tendency of the different precipitates at different annealing conditions, two other samples were designed: (1) a sample with no decomposition of

Al–Mg–Sr and (2) a partially decomposed sample with thick stringers. Details of the tensile test have been described elsewhere [15]. Figure 9 shows clearly how the precipitates of both samples were cracked. The dark crack lines. In Fig. 9a, b are perpendicular to the tensile axis and are the starting points of crack propagation in the Mg matrix [15]. Results indicate that the cracking tendency depends on the thickness (size) of the stringer (precipitate) rather than

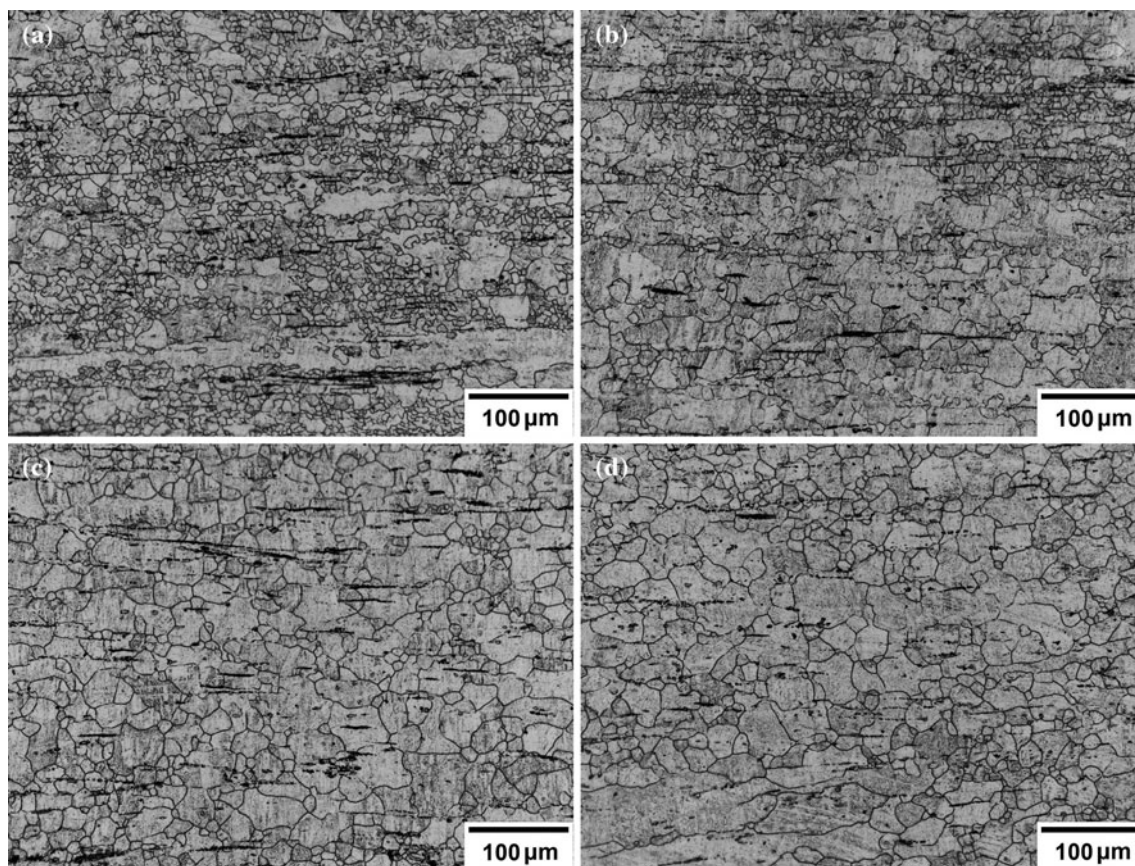


Fig. 5 Optical microstructure of extruded AZ31 + 0.74 wt% Sr. **a** No annealing before extrusion (as-cast), annealed for **b** 10 min, **c** 30 min, **d** 120 min before extrusion

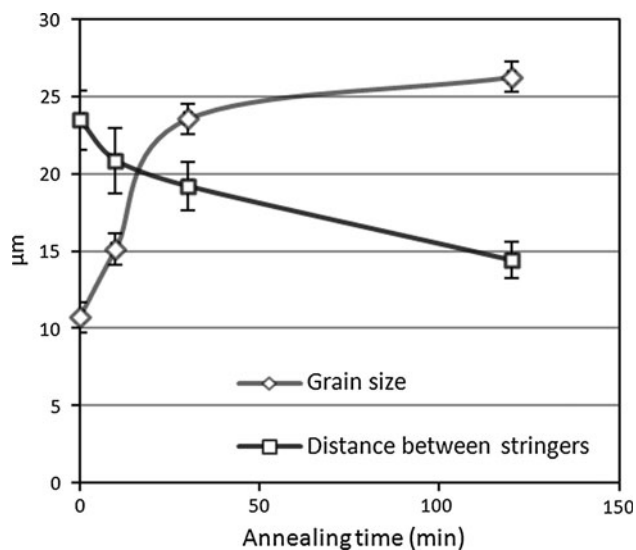


Fig. 6 Grain size of extruded samples vs. annealing time before extrusion

on its composition or morphology. Both Fig. 9a, b reveal that the large precipitates, regardless of their shape and composition, are cracked, while the smaller precipitates have remained unaltered. It has been reported [23] that the

lattice rotation around a precipitate is proportional to the particle size. For non-deformable particles of diameter greater than $\sim 2.5 \mu\text{m}$, lattice rotation in the surrounding matrix is the only relaxation mechanism during deformation. However, for particles in the size range of $0.1\text{--}2.5 \mu\text{m}$, plastic relaxation occurs both by the formation of dislocation loops around the particle and rotated deformation zones [23]. In other words, smaller precipitates develop smaller deformation zones, and the movement of dislocations around them eliminates a portion of the pressure caused by the rotation of the surrounding matrix. However, the large strain accumulation behind the large precipitates imposes a large stress on the particle, and when the stress exceeds a certain level, the precipitate will eventually fracture.

Micro-hardness

Figure 10a shows the Vickers micro hardness distribution across the diameter of the extruded bars. As the annealing time before extrusion increases, the hardness profile becomes smoother. The average hardness values and the average deviation are presented in Fig. 10b. The results indicate that the absolute value of the hardness of the extruded bars is not changed with increasing annealing time,

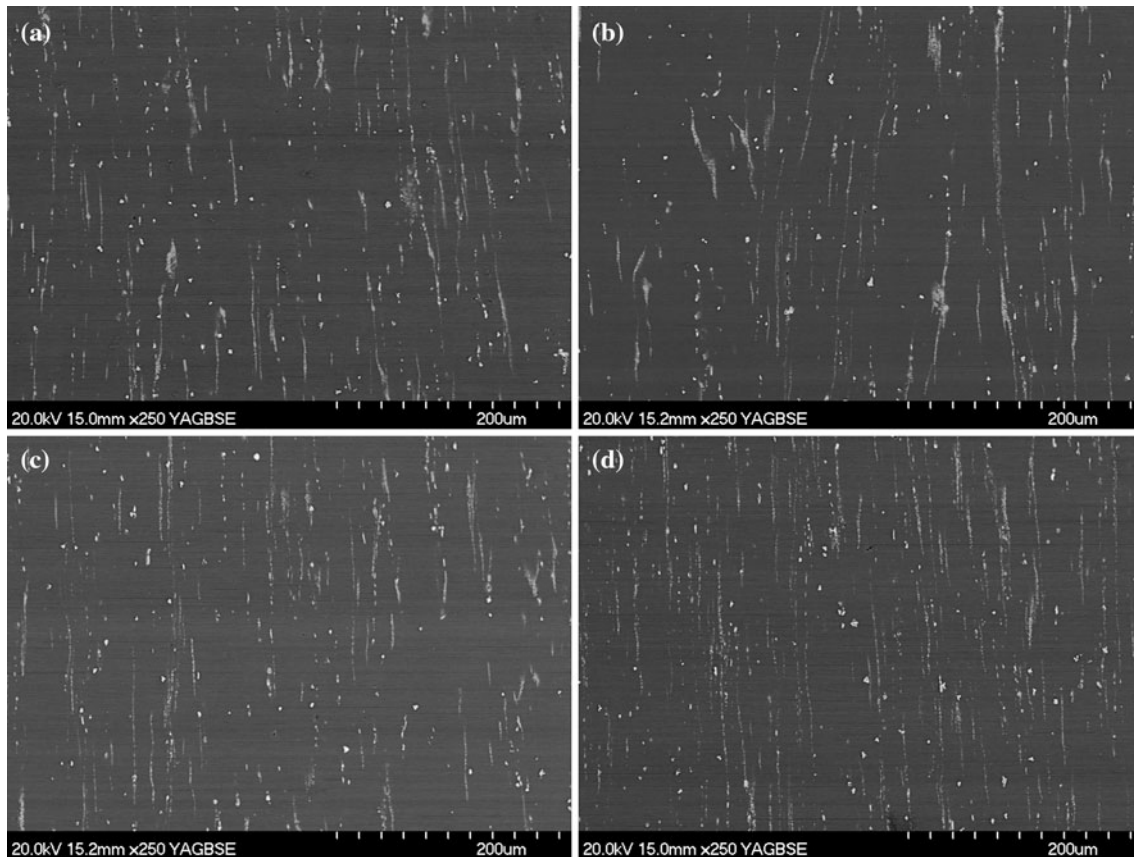


Fig. 7 Back scattered electron images of AZ31 + 0.74 wt% Sr. **a** No annealing before extrusion (as-cast), annealed for **b** 10 min, **c** 30 min, **d** 120 min before extrusion at 300 °C

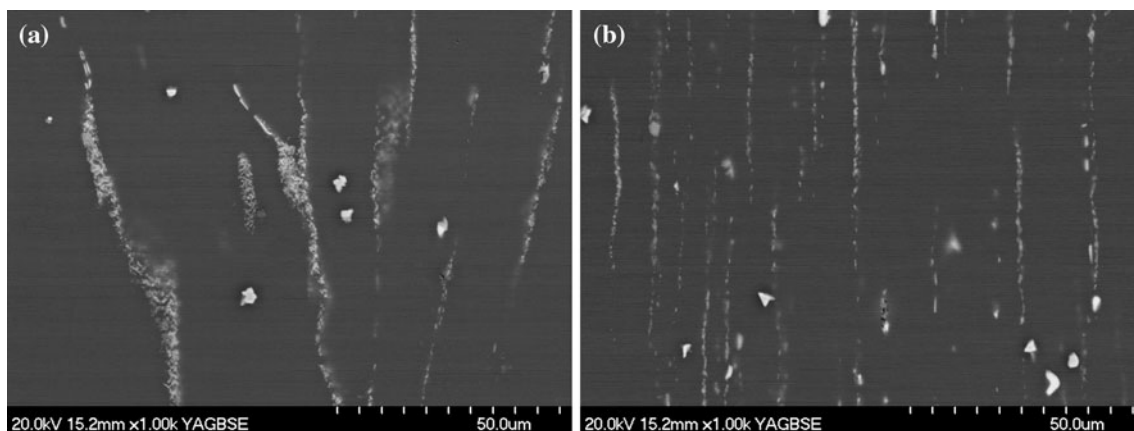


Fig. 8 Back scattered electron images of AZ31 + 0.74 wt% Sr. **a** Annealed for 10 min, **b** 120 min before extrusion

but the deviation is significantly reduced. This also confirms the previous microstructural observations, which indicate the increased homogeneity with increasing annealing time.

Texture

The {0002}, {10-10}, and {11-20} pole figures of extruded samples that have been subjected to different pre-deformation

annealing regimes are shown in Fig. 11. The basal pole figures (first row in Fig. 11) indicate that the ring basal-texture has formed in all samples, but there is no significant relationship between texture intensity/distribution and pre-extrusion annealing. However, the two other rows of pole figures in Fig. 11 reveal notable relationships. The {10-10} pole figures (second row in Fig. 11) show that the increase in annealing time has decreased the maximum intensity of the

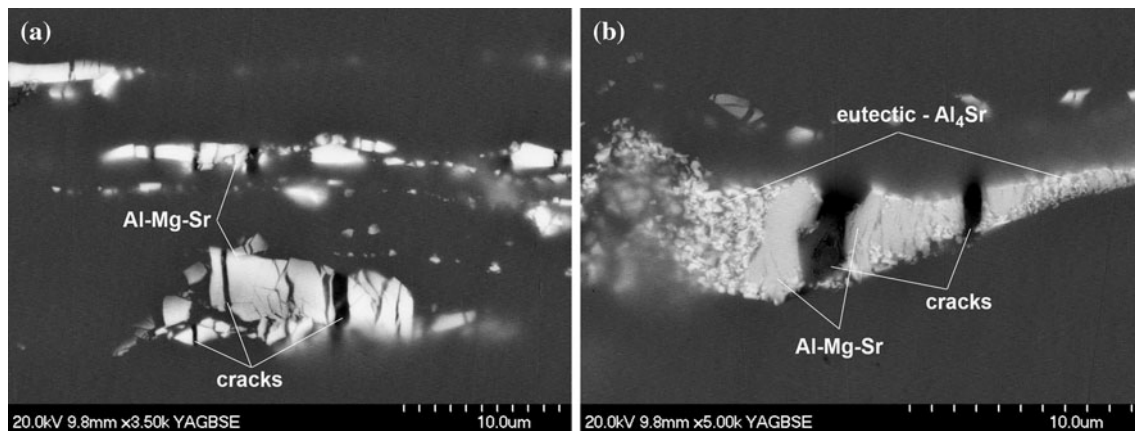


Fig. 9 AZ31 + 0.74 wt% Sr extrusion after tensile test **a** annealed at 250 °C for 30 min and extruded at the same temperature, and **b** annealed at 350 °C for 30 min and extruded at the same temperature

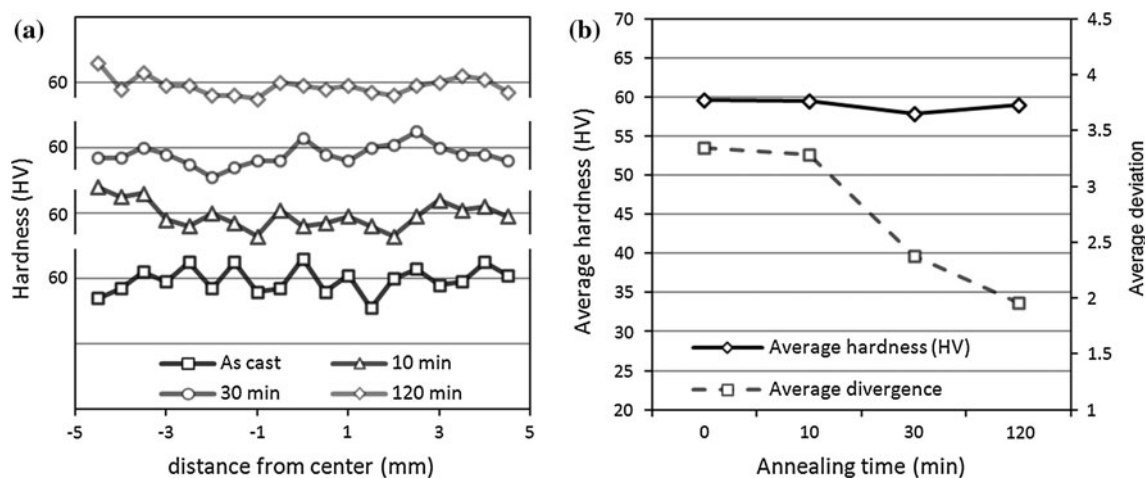


Fig. 10 **a** Hardness distribution, **b** average hardness and average divergence vs. annealing time along the thickness of the extruded bars

pole figures. Moreover, increasing annealing time has weakened the concentration of contours around the ED pole. In the third row of Fig. 11 ($\{11\cdot20\}$ pole figures) show that, when the annealing time has increased, the contours have become more concentrated around the ED axis. The gradual change of texture can be more clearly distinguished in the inverse pole figures presented in Fig. 12. It is observed that increasing the annealing time spreads out the contours from $\{10\cdot10\}$ toward the $\{11\cdot20\}$ corner.

Micro-mechanisms in texture development

The texture measurements indicate that, although the basal texture has not altered, there is a change in the orientation of the crystal plane facing the extrusion direction. To understand which micro-mechanisms are affecting the change in plane orientations, it is necessary to carefully review two main concepts: (1) how dynamic

recrystallization (DRX) develops the basal texture during hot deformation and (2) which slip systems prepare the initial conditions of DRX.

Crystal orientation

(1) As described above, during a deformation process, dislocations slip in differently oriented grains to fulfill the strain compatibility conditions in a polycrystalline microstructure. The slip process is considered in terms of the shear stress resolved on the slip plane in the slip direction (τ). In Mg, the (0002) basal plane and the three $[11\cdot20]$, $[-12\cdot10]$, and $[2\cdot1\cdot10]$ directions prepare the favorable slip systems. As is well known, according to the orientation of the basal planes with respect to the compression axis, different grains would have different resolved shear stresses on the basal system, which could be calculated by the $\tau = \sigma \cos \Phi \cos \lambda$ equation, (where σ is the magnitude of the applied stress, Φ is the angle

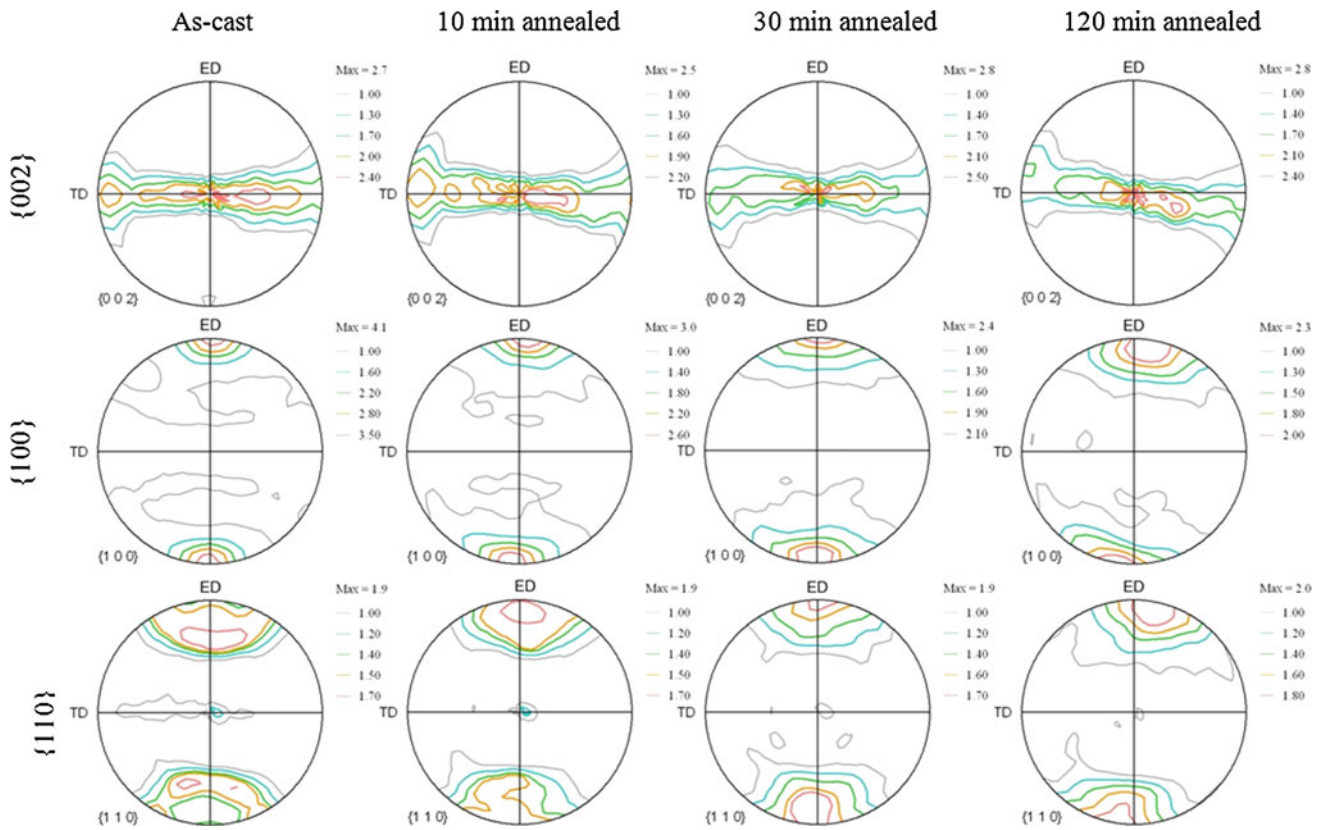


Fig. 11 Pole figure representation of the hot extruded samples having different annealing times prior to extrusion

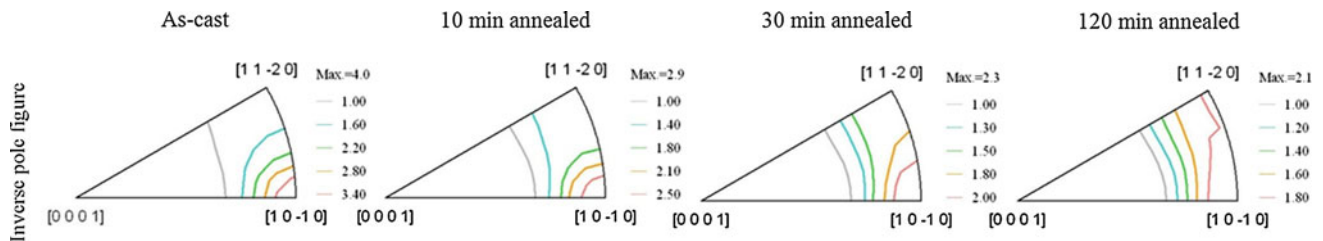


Fig. 12 Inverse pole figures from the circular cross section of the extruded samples having different annealing times before extrusion

between the slip plane normal and the applied stress direction, and λ is the angle between the slip and applied force directions). When the basal plane normal is close to the compression axis, λ would be $\sim 90^\circ$ and τ approaches 0. Consequently there would be limited basal slip in that grain and since the other slip systems in hcp are not activated at moderate temperatures, work hardening would not be sufficient to initiate DRX. Conversely, grains with other orientations where the basal system sees a finite τ would be work-hardened and then transformed, via DRX, to new grains with different orientations. Once again the grains with the basal plane facing the compression axis would stay stable and the others would be consumed via DRX. This cycle would be repeated until all the structures become comprised of grains with the basal normals in the compression direction.

(2) With respect to the second question as to which directions in the basal plane are responsible for dislocation slip (and how they affect the final texture), it can be noted, as before, that there are three favorable slip directions in the basal plane [11-20], [-12-10], and [2-1-10]. In Fig. 13a, the directions are shown in a hexagonal lattice. The [-1100] direction can be described entirely as a combination of slip in the two [11-20] and [2-1-10] directions. In Fig. 13b, c, the slip directions and perpendicular planes perpendicular are presented. If the movement of dislocations on the basal planes in the (11-20) directions becomes restricted, the first order prismatic planes ((10-10) planes) would face the extrusion direction (Fig. 13b). However, if the movement of the (0002)[-1100] system is blocked, the second order prismatic planes ((11-20) planes) would become perpendicular to the extrusion direction (Fig. 13c). The two final

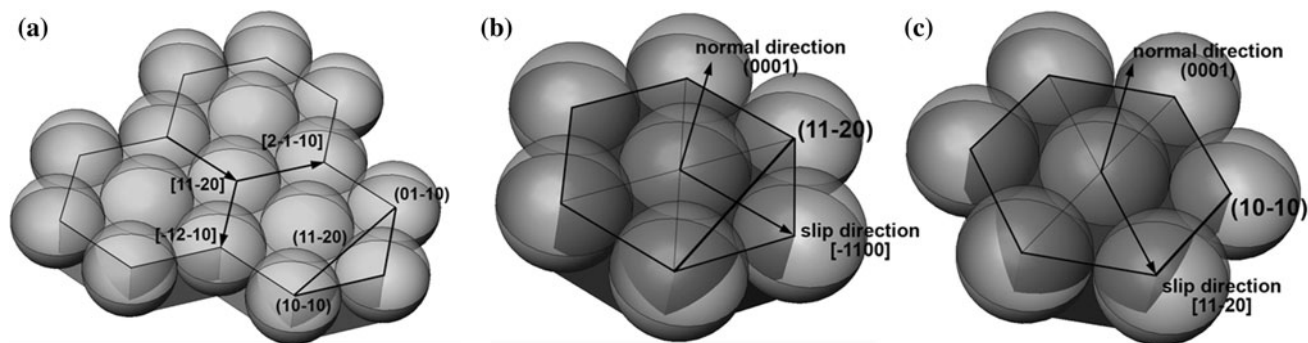


Fig. 13 Favorable slip directions in the basal planes, **b** activation of the (0002)[11-20] slip system and **c** activation of the (0002)[-1100] system

orientations resulting from basal slip blockage in different directions have 30° deviation from one another (Fig. 14a). The priority of activation of slip in the two different directions is based on a simple concept. To move a dislocation one step forward on the basal plane in the [11-20] direction only one atomic jump is enough, while one step movement in the [-1100] direction needs two jumps, one in the [-12-10] direction and the other in [2-1-10] (Fig. 13a). Obviously, slip in the [-1100] direction becomes more energy consuming and would be less favorable.

Lattice resistance

The crystal orientation is not the only controlling parameter in the movement of dislocations. Lattice resistance against dislocation movement is another limiting factor in dislocation motion. In the samples studied, the Al concentration in Mg solid solution (α -Mg) plays a key role in controlling

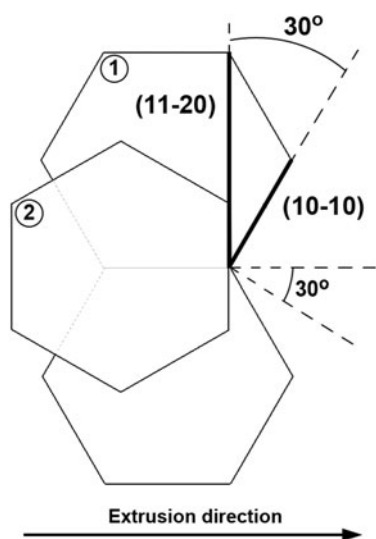


Fig. 14 Schematic view showing the 30° misorientation between the (10-10) and (11-20) planes in a hexagonal crystal

the lattice resistance [13, 14]. As described above, the initial precipitate which forms during solidification of the AZ31 + 0.74Sr alloy is a non-equilibrium Al–Mg–Sr phase. During annealing, this phase rejects its excess Mg and absorbs Al from its surrounding matrix to reach the stable Al_4Sr stoichiometry [7, 15, 21]. The diffusion of Al atoms to the precipitates lowers the level of dissolved Al in α -Mg [15, 21] and it directly affects the lattice resistance against dislocation motion [13, 14]. Consequently, slip becomes easier and the dislocations are able to move in the active slip direction.

In the non-annealed sample, when the c-axis of the grains is close to the compression axis, dislocation movement is restricted by the high lattice resistance even for the “single jump” [11-20] direction. As a result, there would be little or no work hardening in the grain; DRX would not occur and the grain stays stable until the end of deformation. The longer the duration of annealing, the lower is the lattice resistance and the easier is the dislocation motion in the “single jump” directions. Therefore, work hardening followed by DRX occurs in grains, which have the orientation of Fig. 12b. However, dislocations are stopped in grains in which the [-1100] slip direction is needed to fulfill the strain compatibility criteria. This is why the inverse pole figure (IPF) intensity decreases and the contours shift toward the (11-20) corner in Fig. 11 when the annealing time is increased.

The local misorientation in grains could be calculated by measuring the kernel average misorientation (KAM) using EBSD. For a given data point, KAM is the average misorientation between the data point and all of its neighbors (excluding misorientations greater than some prescribed value -5° in this case). In Fig. 15, KAM distribution is plotted separately for grains having their (11-20) and (10-10) planes facing the extrusion direction (the basal poles are in the radial direction for both types of grains). It could be seen how the (11-20) grains illustrate a higher misorientation in very low angles ($<1^\circ$), which is a result of the resistance against easy slip.

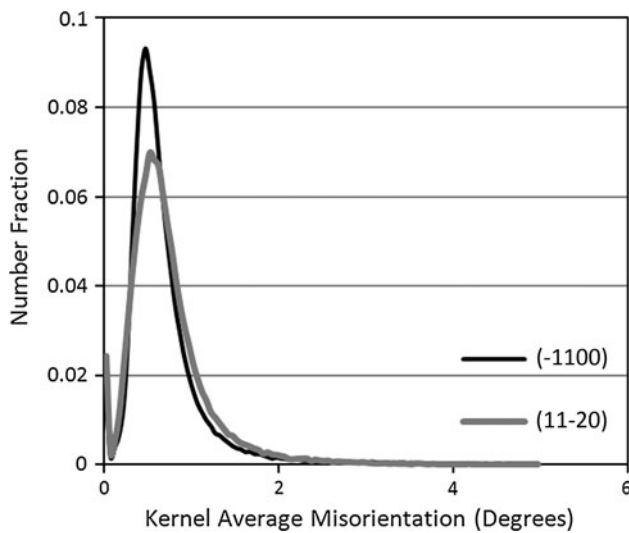


Fig. 15 Kernel average misorientation distribution across the grains having their (11-20) and (-1100) plane facing the extrusion direction

Quantitative analysis of texture change

The texture change could be more quantitatively analyzed by measuring the volume fraction of the first and second order prismatic planes less than 15° away from facing the extrusion direction (f_v), as shown in Fig. 16. It is interesting to see that the volume fraction of (10-10) normals facing the extrusion direction has decreased with increasing annealing time, while the volume fraction of the (11-20) planes perpendicular to extrusion direction has increased. The results show a 30 % decrease in the f_v of the (10-10) and 20 % increase in the (11-20) planes.

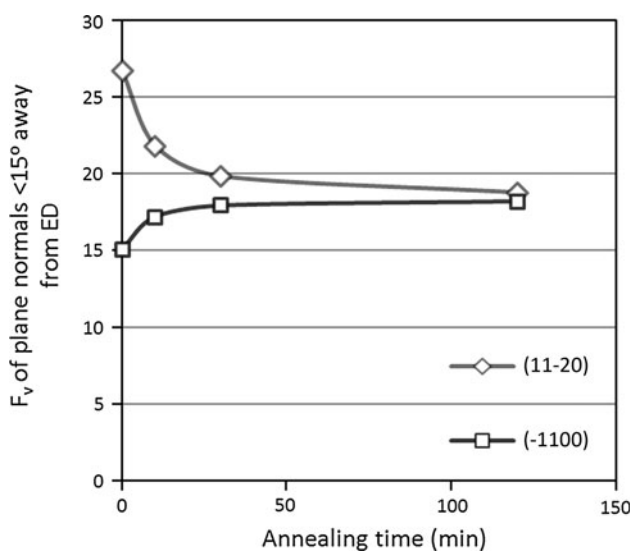


Fig. 16 Volume fraction of the (11-20) and (-1100) normals less than 15° away from extrusion direction vs. annealing time

The competition between slip in the two [11-20] and [-1100] directions has resulted in similar effects in other studies as well. Yi et al. [24] have previously seen a similar change of texture in AZ31 alloys as a result of annealing after extrusion. They have reported that the texture component in the IPF moves from the (10-10) to the (11-20) corner with increasing post-annealing time. Their EBSD results have proven that the driving force for growth of (10-10) grains is diminished in early stages of annealing whereas, (11-20) grains grow extensively and affect the final texture [24]. The reason for why there is a higher driving force for (11-20) grains in Yi’s research [24] can be related to the same factors described here. The lower amount of dislocation movement in the (0002)[-1100] slip system accumulates lower amount of work hardening in the grains facing the (11-20) plane toward the extrusion direction. Consequently, the new grains having this (11-20) orientation would have lower dislocation density and a higher driving force to grow during annealing. Finally, the texture would be dominated by the grain orientations with second prismatic planes facing the extrusion direction.

Conclusions

AZ31 + 0.74Sr alloy was cast and subsequently extruded at 300 °C. The samples were annealed at 400 °C for 10, 30, and 120 min before extrusion and were compared with the sample without annealing. Microstructural analysis, mechanical characterization, and texture measurements have been employed to investigate the effect of annealing before extrusion on the Sr containing AZ31 alloy and the following conclusions are drawn:

1. Annealing at 400°C results in the decomposition of the Mg–Al–Sr non-equilibrium phase to a stable Al₄Sr precipitate. Increasing the annealing time increases the extent of the transformation.
2. Increasing annealing time causes the stringers to disperse more homogeneously and leads to a more uniform hardness gradient across the diameter of the extruded bar.
3. When the annealing time before deformation is increased, stringer particles form in smaller size and more dispersed; in parallel, the reduced solid solubility of Al in α-Mg lowers the resistance to grain growth after recrystallization; consequently, a larger grain size is formed.
4. Although the basal texture is maintained in all annealing conditions studied, with increasing annealing time, there is a slight and gradual change in the plane facing the extrusion direction from first order to second order prism.

5. The change in basal orientation has been attributed to the change in the resistance to dislocation motion in different slip systems. In grains having a basal τ close to zero, the favorable (0002)[11-20] systems experience lower resistance to slip when the amount of Al solute is reduced in α -Mg during annealing. However, the (0002)[-1100] system which consumes higher energy still avoids dislocation motion, work hardening, and DRX. Consequently, maximum intensity of inverse pole figure drops and the volume fraction of (11-20) planes facing the extrusion direction increases.

Acknowledgements This study was carried out under a Strategic project grant from the Natural Sciences and Engineering Research Council (NSERC) of Canada. The authors acknowledge Applied Magnesium (formerly Timminco) for the industrial support and for providing the raw materials and master alloy. Thanks are due to Scott Shook of Applied Magnesium for technical support and to Pirre Vermette of McGill University for assistance in experimental work. One of the authors, A. Sadeghi gratefully acknowledges the financial support of McGill University through MEDA (McGill Engineering Doctoral Award) program.

References

- Luo A, Pekguleryuz MO (1994) *J Mater Sci* 29(20):5259. doi: [10.1007/BF01171534](https://doi.org/10.1007/BF01171534)
- Rokhlin LL (2003) *Magnesium alloys containing rare earth metals: structure and properties*, 1st edn. CRC Press, Boca Raton
- Baril E, Labelle P, Pekguleryuz MO (2003) *J Met* 55(11):34
- Pekguleryuz MO, Kaya AA (2003) *Adv Eng Mater* 5(12):866
- Pekguleryuz MO, Kaya AA (2003) *Magnesium alloys and their applications*, Deutsche Gesellschaft für Materialkunde (DGM), Garmisch, p 74
- Sadeghi A, Pekguleryuz M (2010) Precipitation during the solidification of Mg-3 wt%Al-1 wt%Zn-(0.001–1%)Sr alloys. American Foundry Society annual congress, Orlando, USA
- Sadeghi A, Pekguleryuz M (2011) *J Mater Res* 26:896. doi: [10.1557/jmr.2010.75](https://doi.org/10.1557/jmr.2010.75)
- Sadeghi A, Pekguleryuz M (2011) *Mater Charact* 62(8):742. doi: [10.1016/j.matchar.2011.05.006](https://doi.org/10.1016/j.matchar.2011.05.006)
- Zeng X, Wang Y, Ding W, Luo AA, Sachdev AK (2006) *Metall Mater Trans A* 37(4):1333
- Jing B, Yangshan S, Shan X, Feng X, Tianbai Z (2006) *Mater Sci Eng A* 419(1–2):181
- Jing B, Yangshan S, Feng X, Shan X, Jing Q, Weijian T (2006) *Scripta Mater* 55(12):1163
- Zhao P, Wang Q, Zhai C, Zhu Y (2007) *Mater Sci Eng A* 444(1–2):318
- Sadeghi A, Pekguleryuz M (2011) *Mater Sci Eng A* 528(3):1678
- Sadeghi A, Hoseini M, Pekguleryuz M (2011) *Mater Sci Eng A* 528(7–8):3096. doi: [10.1016/j.msea.2010.12.091](https://doi.org/10.1016/j.msea.2010.12.091)
- Sadeghi A, Shook S, Pekguleryuz M (2011) *Mater Sci Eng A* 528(25–26):7529. doi: [10.1016/j.msea.2011.06.060](https://doi.org/10.1016/j.msea.2011.06.060)
- Huppmann M, Lentz M, Chedid S, Reimers W (2009) *J Mater Sci* 46(4):938. doi: [10.1007/s10853-010-4838-0](https://doi.org/10.1007/s10853-010-4838-0)
- Chen Y, Wang Q, Peng J, Zhai C, Ding W (2007) *J Mater Process Technol* 182(1–3):281
- Ye Lapovok R, Barnett MR, Davies CHJ (2004) *J Mater Process Technol* 146(3):408
- Zhu S-Q, Yan H-G, Xia W-J, Liu J-Z, Jiang F-F (2009) *J Mater Sci* 44(14):3800. doi: [10.1007/s10853-009-3513-9](https://doi.org/10.1007/s10853-009-3513-9)
- Janz A, Mirković D, Gröbner J, Jun Zhu, Chang YA, Schmid-Fetzer R (2007) *Intermetallics* 15:506
- L'Espérance G, Plamondon P, Kunst M, Fischersworing-Bunk A (2010) *Intermetallics* 18(1):1
- Becerra A, Pekguleryuz M (2009) *J Mater Res* 24(5):1722. doi: [10.1557/JMR.2009.0205](https://doi.org/10.1557/JMR.2009.0205)
- Humphreys FJ, Hatherly M (1996) *Recrystallization and related annealing phenomena*. Pergamon Press, Oxford
- Yia S, Brokmeier H, Letzig D (2010) *J Alloy Compd* 506:364